RSC Advances

ROYAL SOCIETY OF CHEMISTRY

www.rsc.org/advances

Cite this: DOI: 10.1039/c0xx00000x

www.rsc.org/xxxxxx

ARTICLE TYPE

Facile synthesis of size and wavelength tunable hollow gold nanostructures for the development of a LSPR based label-free fiber-optic biosensor

Jitendra Satija,[a,b] Joseph Tharion[a] and Soumyo Mukherji*[,a,c,d]

Received (in XXX, XXX) Xth XXXXXXXXX 20XX, Accepted Xth XXXXXXXXX 20XX
DOI: 10.1039/b000000x

Hollow bimetallic nanostructures have recently emerged as attractive plasmonic materials due to the ease of optical tunability by changing their size/composition. Currently available methods, in addition to being tedious and time-consuming, result in polydispersed nanostructures, particularly due to polydispersed templates. In this study, optically tunable hollow gold nanostructures (HGNS) were synthesized by galvanic replacement reaction between silver nanospheres (AgNS) templates and gold salt. Monodispersed AgNS were created using a gold seed-mediated heteroepitaxial growth. Since it is easier to ensure monodispersed gold nanosphere seeds, the resulting AgNS showed a tight control on size. Hollow gold nanostructures 43 – 70 nm in size with extinction maxima ranging between 450 – 590 nm were produced by varying the gold to silver molar ratio. The nanostructures were observed to be monodispersed and uniform (SD ≤11%) in all the batches. Furthermore, the synthesized HGNS were immobilized on dendrimer-functionalized U-shaped fiber-optic probes to develop a localized surface plasmon resonance (LSPR) based sensor. Refractive index sensitivity of the HGNS based sensors was found to be 1.5-fold higher than solid gold nanosphere (GNS)-based fiber-optic sensors. These HGNS-based fiber-optic probes were subsequently used to develop an immunosensor with improved sensitivity by using human immunoglobulin-G (HIgG) as receptor molecules and goat-anti-HIgG as a target analyte.

Introduction

Localized surface plasmon resonance (LSPR) is a long-studied nanoscale phenomenon of metal nanoparticles which creates sharp spectral extinction peaks as well as strong electromagnetic near-field enhancement due to collective oscillations of electrons. [1] During the past decade, prodigious efforts have been devoted to develop ultra-sensitive, point-of-care biosensing devices using LPSR.[2-4] Since LSPR is very sensitive to size, shape and composition of the nanoparticles, numerous label-free sensing schemes have been developed using the nanoparticles of different metals such as gold, silver, platinum and copper, and different shapes such as nanorods,[5,6] nanoshells,[7,8] nanostars,[9] nanobipyramids,[10,11] and bimetallic nanostructures,[12] to name a few. Some of these nanostructures have shown significant improvement in sensor performance, especially with reference to detection limit towards target analytes, which is associated with high extinction coefficient, higher wavelength of absorption and dielectric sensitivity of the nanostructures.[13]

Recently, hollow metallic nanostructures have garnered interest for use in label-free optical biosensor development due to their near infra-red peak absorption wavelength and high extinction coefficient.[12] Unlike gold nanorods, their size can be controlled more easily and their surface can be functionalized using well established thiol chemistry.[5] The optical properties of hollow metallic nanostructures can be precisely and systematically tuned over a broad range of wavelengths by controlling the hollow cavity to shell thickness ratio.[14] In addition, the plasmonic properties of these hollow metallic nanostructures are sometimes superior compared to their solid counterparts.[15]

Typically, hollow metallic nanostructures are synthesized by galvanic replacement reactions.[16,17] The template metal nanoparticles are galvanically replaced by the metal ions in solution, which gets reduced and is deposited forming a shell, resulting in a hollow or partially hollow interior cavity. This replacement reaction happens only when the core metal has lower redox potential than the metal of the outer shell layer. For example, silver (Ag^+/Ag 0.8V) has a lower redox potential than gold ($AuCl_4^-$/Au 0.99V). Thus, addition of gold salt solution to silver colloids oxidizes the silver atoms and creates small pinholes and cavities in silver nanospheres, which progressively increase in size as the molar ratio of gold to silver is increased.[14] This strategy has been used to develop various hollow metallic nanostructures, including Au/Ag shell/core nanoparticles,[14] Pd/Au shell/core nanoparticles,[18] and Pt/Ag shell/core nanoparticles.[19]

Most of the earlier studies centred on the establishment of innovative strategies to create hollow nanostructures.[14-17,20]

However, important parameters, such as monodispersity, colloidal stability, reproducibility and biocompatibility which play a critical role in biomedical applications were not adequately addressed. In addition, some of these preparation methods were found to be tedious and time-consuming. For example, Xia and coworkers developed anisotropic hollow gold nanocages by galvanic replacement reaction but that chemical method makes use of some toxic reagents.[16,21] Thereby, surface engineering of such nanocages is essential prior to their *in-vivo* applications, which makes the process tedious and expensive. Another approach, in which gold nanoshells are prepared by sacrificing cobalt nanoparticles, requires stringent oxygen-free ambience to prevent oxidation of cobalt prior to galvanic replacement reaction.[22] Prevo *et al*. (2008) reported a green approach for synthesis of hollow gold nanoshells by galvanic replacement reaction of AgNS templates.[17] However, this method yielded polydispersed nanostructures which are usually not suitable for plasmonic sensor applications. These major challenges are yet to be addressed.

In this study, we have developed a systematic approach to synthesize uniform, monodispersed and highly stable hollow gold nanostructures (HGNS). Unlike previously reported methods for synthesis of hollow gold nanostructures, the current method involves three simple steps. This protocol neither requires any heating and/or reflux conditions nor any pre-preparation of gold salt solution. The only controlling parameter is the molar ratio of gold to silver which makes this method advantageous for commercial applications. Since the monodispersity of HGNS is dictated by template nanoparticles, a heteroepitaxial growth approach was used to produce AgNS of uniform size and shape. As the lattice mismatch between gold and silver is only 0.25%, gold nanoparticles of very small size were used as seed to grow silver on their surface.[23] Following the preparation of AgNS, size and wavelength tunable HGNS were produced by modulating the gold to silver molar ratio. The whole synthesis procedure involved moderate mixing of the reagents at room temperature. After detailed characterization, the potential of HGNS in the development of LSPR based label-free immunosensor was attempted. An absorption-based U-shaped fiber-optic biosensor was used for this study because of their (i) high sensor performance, ii) immunity to interference from molecules in the bulk of the sample, (iii) simplicity of design and (iv) ease of fabrication.

Materials and Methods

Materials

Fourth generation polyamidoamine (PAMAM) dendrimer (64 terminal amine groups), 1,1' carbonyldiimidazole (CDI), 11-mercapto undecanoic acid (MUA), phosphate buffer saline (PBS, 10 mM and pH 7.4), silver nitrate ($AgNO_3$) and tetra chloroaurate ($HAuCl_4$) (99.99% pure, 30 wt. % in dilute HCl) were purchased from Sigma-Aldrich, India. N-hydroxysuccinimide (NHS) and l-ethyl-3-(3-dimethylaminopropyl) carbodiimide (EDC) were obtained from Fluka, India. Bovine serum albumin (BSA), Human Immunoglobulin G (HIgG), Goat anti-Human Immunoglobulin G (GaHIgG) and Rabbit Immunoglobulin G (RIgG) were procured from Bangalore Genei, India. Ammonia solution, glucose, sodium hydroxide, tetrakis(hydroxymethyl) phosphonium chloride (THPC, 80%), sodium dodecyl sulfate (SDS) and 1,4-dioxane were purchased from Merck, India. Optical fibers of 200 µm core diameter were obtained from Ceramoptec, United States. All glassware were thoroughly cleaned with aqua regia (3:1 = HCl:HNO_3) followed by extensive rinsing with milliQ water (>18 MΩ resistivity) prior to nanoparticles synthesis.

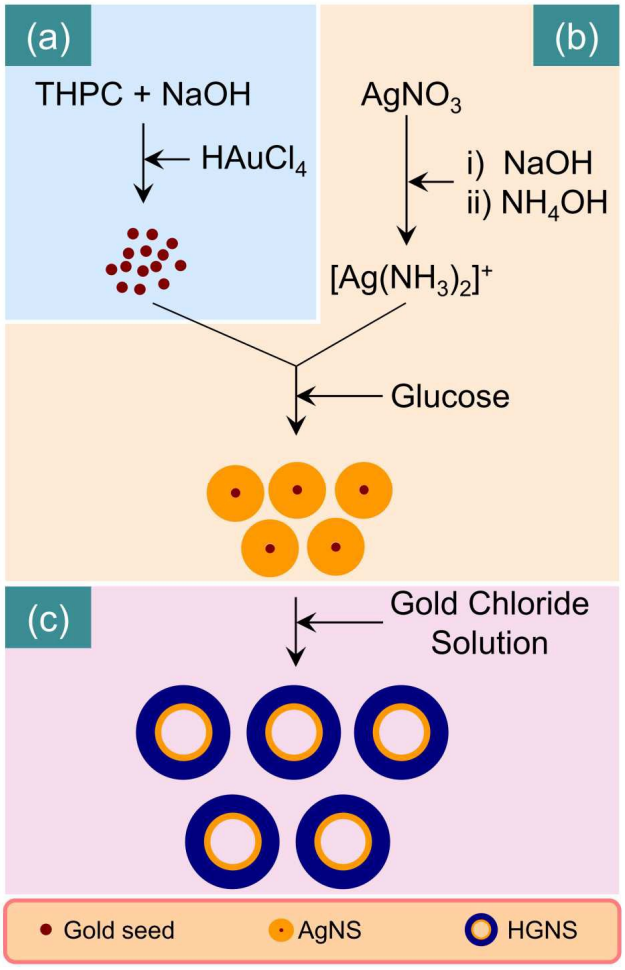

Fig. 1 Schematic representation of the three step method for the synthesis of hollow gold nanostructures (HGNS); a) synthesis of gold seed particles, b) synthesis of silver nanospheres by heteroepitaxial growth method using gold seed particles, and c) preparation of HGNS by galvanic replacement reaction between template AgNS and gold salt solution.

Synthesis of HGNS

HGNS were synthesized in three steps by galvanic replacement reaction between template AgNS and gold salt solution as shown in Fig.1.

Step I: Preparation of gold seeds

Gold seed particles were prepared by reducing gold (III) chloride salt solution with alkaline solution of THPC (See ESI, S1†).[24] Extinction spectra of gold seeds exhibited a small hump at ~500 nm, which is the characteristic feature of very small size gold nanoparticles (Fig. S1a).[25,26] FEG-TEM micrograph confirmed the formation of spherical shaped nanoparticles of 2.1 ± 0.6 nm (n>100) (Fig. S1b).

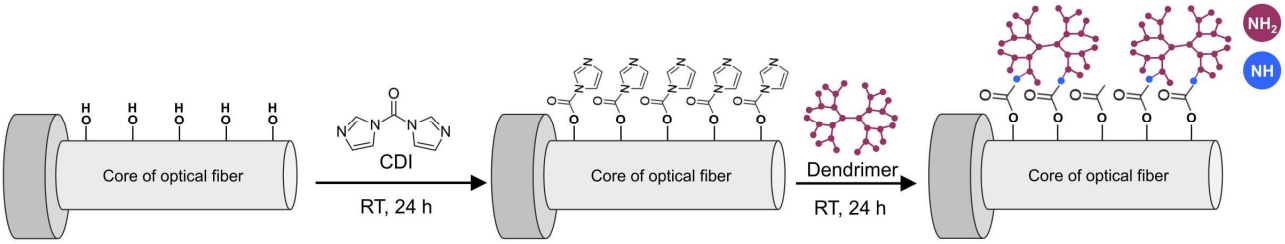

Fig. 2 Schematic representation of dendrimer immobilization protocol on fiber-optic sensor platform using CDI linker.

Step II: Synthesis of silver nanospheres

Silver nanospheres were produced by heteroepitaxial growth method by growing silver on gold seeds using Tollens' reaction, i.e. glucose mediated reduction of diamine silver complex ($[Ag(NH_3)_2]^+$).[23,27] First, 65 µL of sodium hydroxide (1 M) was mixed with 15 mL of freshly prepared aqueous silver nitrate solution (1 mM), which immediately formed a dirty grey colored precipitate. To this, 25 µL of freshly prepared aqueous ammonia solution (6.25% v/v) was added which instantly dissolved the precipitate to give a clear solution, indicating the formation of diamine silver complex (DSC). The chemical reactions and balanced stoichiometric equations are explained in S2† in ESI. To prepare AgNS, 5 µL of gold seed solution was added to 8 mL of freshly prepared DSC solution. To this stirred mixture, 320 µL of freshly prepared glucose solution (conc. = 36 mg/mL) was added. The change in the color of the solution to yellow within a few seconds indicates the formation of silver colloids. The mixture was stirred for another 2 mins and then stored at 4°C.

Extinction spectra of AgNS exhibited a sharp absorption peak at 409 nm with a narrow full width at half maximum (FWHM) of 62 nm (See ESI, Fig. S2†). FEG-TEM observations revealed the formation of spherical shaped AgNS with the average diameter of 35.6 ± 3.8 nm (n >100) (See ESI, Fig. S3†). Ellipticity of the nanoparticles (calculated by taking the ratio of size of long axis to short axis of nanoparticles) was found to be 1.12 ± 0.08, indicating the near spherical shape of AgNS. The tight control on size and shape distribution of AgNS was due to the monodispered nature of gold seed particles.

Step III: Synthesis of hollow gold nanostructures

HGNS were synthesized by galvanic replacement reaction between AgNS and gold salt solution. A 2 mL of the as-prepared AgNS colloidal solution was mixed with 1 mL of aqueous solution of SDS (conc. = 1 mg/mL) and the mixture was diluted up to 20 mL with DI water. The SDS surfactant provided the stability to the nanostructures and prevented aggregation.[28] To the above mixture, 140 µL of NaOH solution (1M) was added in order to increase the pH to 10.5. This alkaline medium is required to convert $AuCl_4^-$ ions into the more reactive ionic species, i.e. $AuCl_2^-$, which has higher reduction potential.[29]

Finally, 5 mL of aqueous solution of gold chloride (III) salt (of varying concentration, i.e. 72, 145, 217, 289, 434, 867 µM, to get different batches) was added at a slow rate of 30 µL/min using a syringe pump (Harvard Pump 22, Instech Laboratories, Inc, Netherlands). This resulted in six different batches of HGNS with gold to silver molar ratio ranging from 0.17 to 2.0 (See ESI, table S1†). The term '$HGNS_x$' used in this article defines the HGNS type in which 'x' represents the molar ratio of gold to silver. After completion of the reaction, the resultant mixtures were stirred for an additional 10 mins and then stored at 4°C. All the colloidal solutions of HGNS were characterized by UV-Vis spectroscopy and FEG-TEM (JSM-7600F, JEOL; See ESI, S3†).

Fabrication of LSPR based fiber-optic sensor using HGNS

To design LSPR based label-free sensors, U-shaped fiber-optic probes were used in this study because of their ergonomic design and high sensitivity compared to other geometrical designs.[30-32] The fabrication procedure and parameters optimized for LSPR based U-shaped fiber-optic probes have been described earlier by our group.[33,34] Briefly, the fiber-optic probe was fabricated using 200 µm core diameter and the bending diameter and probe length were kept to 1.5 mm and 2 cm respectively. Thereafter, the probes were cleaned and functionalized with PAMAM dendrimer to generate amine groups on the sensor surface which helps in binding of HGNS. The dendrimer molecules offer comparatively larger surface area by creating a three-dimensional matrix with controlled distribution of the nanostructures on the sensor surface compared to conventionally used linkers.[35,36]

For cleaning, all the probes were dipped in methanol-HCl mixture (1:1 v/v) for 60 mins followed by thorough rinsing with DI water. The probes were incubated in conc. H_2SO_4 for 60 mins followed by exhaustive rinsing with DI water. Thereafter, these were treated with sulfochromic acid (2.5 mg of $K_2Cr_2O_7$ dissolved in DI water and 100 mL of concentrated H_2SO_4) for 10 mins to generate surface hydroxyl groups and washed thoroughly with DI water and dried under nitrogen. The probes were then heated in a hot air oven at 110°C for 60 mins to remove adsorbed water from the surface. The cleaned fiber probes were activated by dipping into CDI solution (80 mM, prepared in 1,4-dioxane) for 24 h at room temperature. CDI reacts with hydroxyl (–OH) groups of glass surface and forms amine-reactive imidazole carbamate groups. The activated fiber probes were washed thrice with dioxane. Amine-terminated PAMAM dendrimer was immobilized on fiber-optic probes using CDI as linker molecules by incubation in PAMAM dendrimer solution (20 µM in DI water) for 24 h (Fig. 2).[35,37] Amine groups of the dendrimer form covalent carbamate linkage directly on CDI activated glass fiber surface. Thereafter, fiber probes were washed thrice with DI water and dried using flowing nitrogen gas.

HGNS were immobilized on PAMAM dendrimer-functionalized fiber-optic probes by incubating the sensing region in a colloidal solution of HGNS. The binding kinetics of HGNS on fiber-optic probes were monitored in real-time by recording the change in absorption at peak plasmonic wavelength (at a regular interval of 5 sec) using an optical set-up (See ESI, S4†). Thereafter, the HGNS immobilized probes were evaluated for refractive index (RI) sensitivity by using sucrose solution of

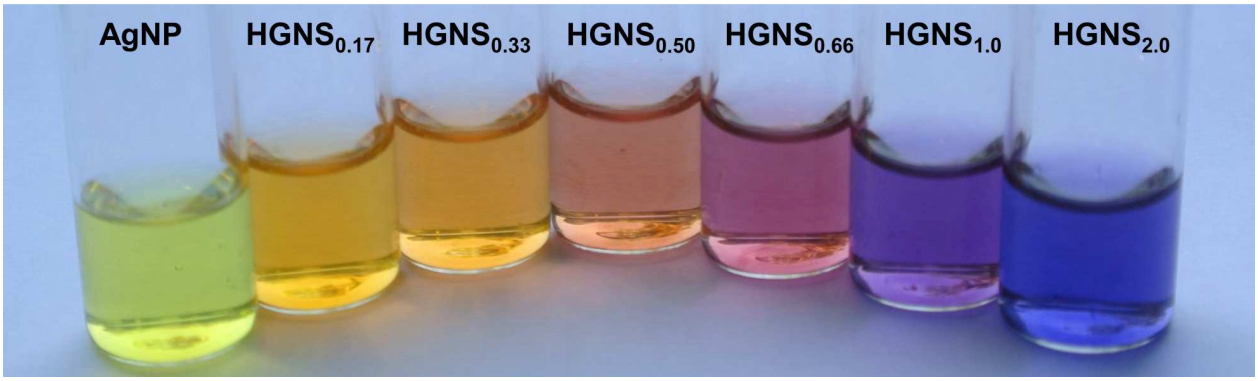

Fig. 3 Photograph of aqueous colloidal solution of silver nanospheres and different hollow gold nanostructures batches prepared with different molar ratios of gold to silver. The term 'HGNS$_x$' used in this article is to define the HGNS type in which 'x' represents the molar ratio of gold to silver.

varying refractive indices ranging from 1.33 to 1.36. Sucrose solutions of increasing RI values were successively introduced into the flow cell and the absorbance spectra were recorded. RI sensitivity was obtained by measuring the absorbance changes at peak plasmonic wavelength ($\Delta A_{\lambda max}$) in the presence of sucrose solutions of different RI and represented as $\Delta A_{\lambda max}$/RIU.

Preparation of LSPR based label-free biosensor

To demonstrate the potential of HGNS coated fiber-optic probes for label-free biosensor, an immunoassay was carried out using HIgG as the receptor molecule and GaHIgG as target analyte. The HIgG molecules were immobilized on HGNS coated fiber-optic probes following the protocol described as explained earlier by Chiang *et al.* (2010).[38] Firstly, HGNS immobilized fiber-optic probes were incubated overnight in MUA solution (10 mM prepared in ethanol). This treatment creates a layer of MUA with carboxyl functionalities at the surface of HGNS. Thereafter, the probes were washed thrice with ethanol and dried under flowing nitrogen gas. The carboxyl groups of MUA were activated using freshly prepared 1:1 (v/v) aqueous mixture of EDC (400 mM) and NHS (100 mM). These activated probes were washed thrice with DI water and incubated in HIgG solution (conc. = 100 µg/mL) prepared in PBS solution (10 mM, pH 7.4). Thereafter, the probes were washed thrice with PBS solution and followed by BSA treatment (conc. = 2 mg/mL in PBS) for 30 mins. BSA helps in the reduction of non-specific binding by covering the free aldehyde functional groups on the sensor surface.[39] Subsequently, the probes were washed thrice with PBS solution and used immediately for immunosensing.

The receptor-analyte binding experiments were performed real-time and the temporal changes in absorbance spectra were recorded. These could subsequently be used for elucidating the binding kinetics, by observing the variation of absorption at a particular wavelength. The probes were tested for different concentrations of GaHIgG analyte ranging from 1 ng/mL to 15 µg/mL. The sensor probe was incubated first with 1 ng/mL concentration of GaHIgG for 90 mins followed by successively higher concentrations of the analyte. The absorbance measured for buffer solution was taken as background reference in these experiments. The sensor response was recorded at intervals of five seconds. For each concentration, minimum three sets of experiments were performed.

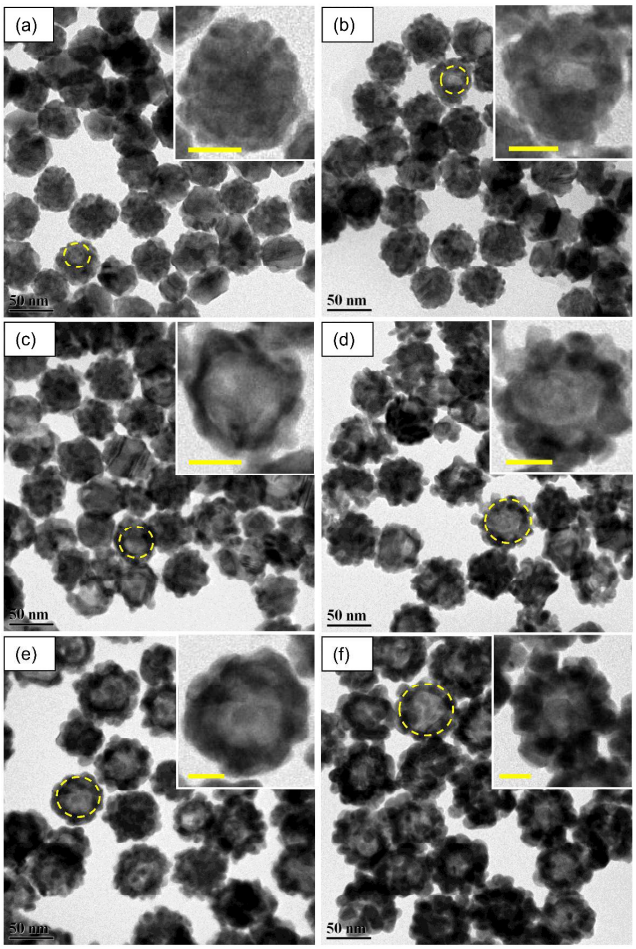

Fig. 4 TEM images of HGNS produced from galvanic replacement reaction between gold salt and silver nanospheres using gold to silver molar ratio of a) 0.17, b) 0.33, c) 0.5, d) 0.66, e) 1.0 and f) 2.0. The circle indicates the presence of hollow cavity in HGNS. Inset image shows the magnified images of an individual HGNS. The scale bar length is 20 nm for all inset images.

Results and Discussion

Synthesis and characterization of HGNS

Fig. 3 shows the photograph of aqueous colloidal solution of AgNS and different batches of HGNS. As the gold to silver molar ratio was increased, greater structural transformation occurred in solid AgNS due to galvanic replacement reaction.

Consequentially, the faint yellow colored AgNS turned orange, pale brown, violet and blue depending upon the gold to molar ratio.

FEG-TEM images of different HGNS batches prepared from various molar ratios of gold to silver are shown in Fig. 4. As shown in the TEM micrographs, all the HGNS batches yielded spherical shaped hollow nanostructures. The hollow cavity could be discerned by noting the difference in contrast between inner and outer regions of the nanostructures (encircled nanostructure in each FEG-TEM image in Fig. 4). At low molar ratio, i.e. 0.17, some pinholes with small hollow cavities were visible only in few nanostructures (Fig. 4.4a). The hollow cavity became distinct in HGNS batches with molar ratio > 0.17 (Fig. 4b-4f). The size of the inner hollow cavity was found to increase with increase in gold to silver molar ratio, due to the higher degree of galvanic silver replacement from AgNS caused by the availability of increased number of gold (III) ions. However, the exact size of hollow cavity could not be measured due to the inability in identifying the boundary between the hollow core and thick shell, which was observed in most nanostructures. Unreacted solid AgNSs were not seen in any of the TEM images which indicate the uniformity of galvanic replacement reaction in all the HGNS batches. Further, no other solid nanostructures, like gold nanoparticles, were observed in any of the HGNS batches which suggest that no parallel nucleation and growth pattern occurred. This is a definite advantage over an earlier method in which formation of solid GNP was observed as a byproduct.[17]

The average particle size was found to increase from 43.7 ± 4.7 nm to 69.4 ± 6.2 nm (Table 1) which was due to the deposition of gold (Au^0) on the surface of AgNS template. For all the HGNS batches, the standard deviation was found to be ≤11%, which suggested the formation of reasonably monodispersed nanostructures. The relatively narrow size distribution is a reflection of AgNS from which the HGNSs were grown. The surface of HGNS appeared to be rough with some rosette features. This morphological characteristic was attributed to poor solubility of silver chloride, which was formed during the galvanic replacement reaction.[29] Since the room temperature solubility product of silver chloride is very low ($\sim 10^{-10}$), concurrent AgCl precipitation occurred while Ag^+ ions were replaced. The precipitate can disrupt the epitaxial deposition of gold and interfere with the inter-diffusion rate between gold and silver. As a result, nanostructures with rosette features and rough surface were produced. Such morphological features may also be ascribed to the presence of surfactant on AgNS which might affect the inter-diffusion rate. This was observed and reported earlier during the surfactant mediated synthesis of silver and gold nanostructures.[28,40] However, the exact mechanism of surfactant directed formation of rough/spiky nanostructures is still unclear.

The energy-dispersive X-ray spectroscopy (EDX) spectra of all the HGNS batches are depicted in Fig. 5. The EDX spectrum confirmed the presence of characteristic peaks of both gold (M_α and L_α at 2.12 and 9.71 keV respectively) and silver (L_α and L_β at 3.05 and 3.20 KeV respectively) elements in all the HGNS batches. The typical peaks for copper and carbon atoms were also observed, which were from the supporting carbon-coated copper grid used for analysis. No signal for chlorine was detected indicating the absence of silver chloride in the HGNS sample, suggesting the efficient washing process of HGNS samples by centrifugation. A progressive increase in percent atomic Au/Ag ratio was observed (Table 1), which is in consistent with the growth model in which gold was deposited on the surface, and silver was partially precipitated out from the interior, giving rise to the formation of a hollow nanostructure.

The intensity normalized extinction spectra obtained from aqueous suspension of AgNS and all HGNS batches are shown in

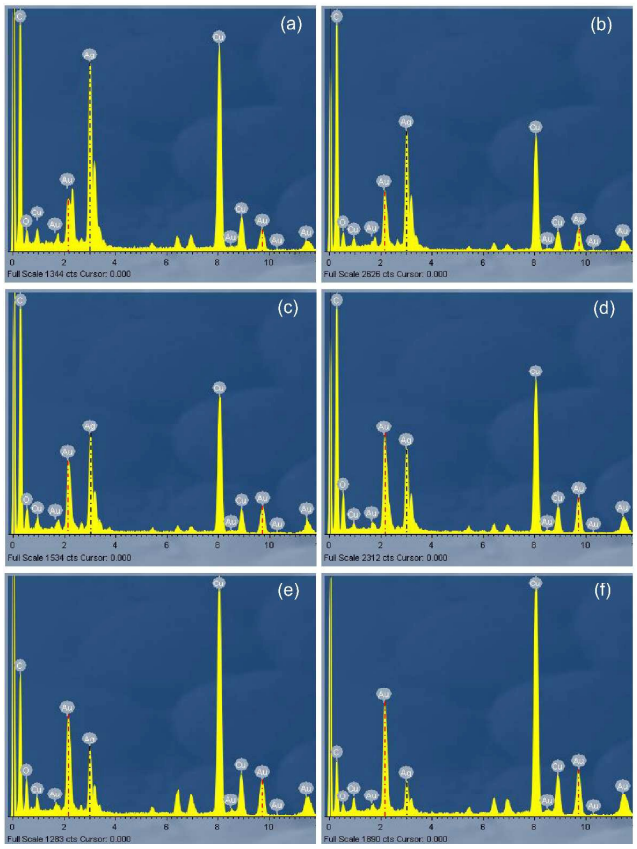

Fig. 5 Energy-dispersive X-ray spectra of HGNS produced from galvanic replacement reaction between gold salt and silver nanospheres using gold to silver molar ratio of a) 0.17, b) 0.33, c) 0.5, d) 0.66, e) 1.0 and f) 2.0. Red dashed line shows the characteristic peaks due to gold (M_α and L_α at 2.12 and 9.71 keV respectively) while the black dashed line shows the silver (L_α and L_β at 3.05 and 3.20 KeV respectively).

Table 1 Morphological and optical properties of hollow gold nanostructures produced with different molar ratio of gold to silver.

HGNS type	Wavelength (nm)	Size ± SD (nm)	Percent Au (from EDX)	Percent Ag (from EDX)	Percent atomic Au/Ag
$HGNS_{0.17}$	450	43.7 ± 4.7	14.2 ± 0.8	85.8 ± 0.8	0.17 ± 0.01
$HGNS_{0.33}$	470	46.8 ± 4.9	23.0 ± 0.9	77.0 ± 0.9	0.3 ± 0.02
$HGNS_{0.50}$	499	49.4 ± 4.3	32.2 ± 2.3	67.8 ± 2.3	0.48 ±0.05
$HGNS_{0.66}$	524	51.8 ± 5.7	37.7 ± 1.8	62.3 ± 1.8	0.61 ± 0.05
$HGNS_{1.0}$	562	55.4 ± 6.0	46.2 ± 0.7	53.8 ± 0.7	1.09 ± 0.08
$HGNS_{2.0}$	587	69.4 ± 6.2	32.6 ± 1.6	67.4 ± 1.6	2.07 ± 0.15

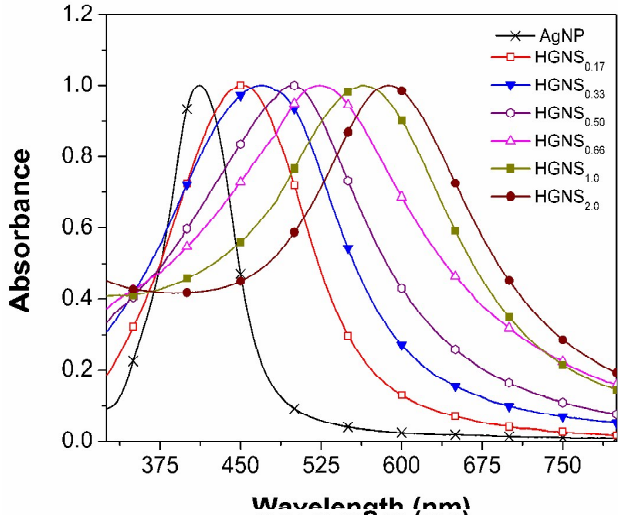

Fig. 6 Intensity normalized extinction spectra of silver nanospheres and various hollow gold nanostructures prepared with different molar ratio of gold to silver.

Fig. 6. The characteristic peak absorption wavelength of AgNS (λ_{max}) was absent in all the HGNS batches, which suggests the galvanic replacement reaction was uniform in all the batches and there were no unreacted AgNS in the resultant colloidal solution. The extinction maxima of HGNS batches showed a wavelength shift from 450 to 587 nm as a function of gold to silver molar ratio. The observed red shift was due to the combined effect of increased size of nanostructures, change in the hollow cavity to shell thickness ratio and the chemical composition of the nanostructures. The extinction peak of HGNS could be precisely tuned over a broad spectral range by controlling gold to silver molar ratio. This behavior is consistent with the morphological and optical properties of hollow nanocages reported by Xia's group.[41,42]

Development of LSPR based fiber-optic sensor

Since the sensitivity of LSPR based sensor is directly proportional to extinction coefficient (which increases with nanoparticle size[43]), and wavelength of absorption maxima,[33,44] $HGNS_{2.0}$, (size ~70 nm, λ_{max} = 587 nm) was used to develop the sensor. Fig. 7a shows the absorbance spectra recorded at different absorbance values (or at different time intervals) during the process of HGNS binding on dendrimer functionalized fiber-optic probes. As the probes were dipped in colloidal solution of HGNS, a characteristic extinction spectrum of HNGS was observed. The extinction intensity increased linearly with incubation time indicating the continuous binding of HGNS on the sensing surface (Fig. 7b). The peak absorbance of spectrum reached ~3 units within 15 mins of incubation. Above an absorbance of ~3 units, low signal to noise ratio (SNR) was observed due to the high absorption of light at the peak extinction wavelength of HGNS, resulting in a noisy signal (Fig 7a). Hence, to limit the absorbance value, further HGNS binding was stopped by flushing DI water in the flow cell.

The spectral characteristics of HGNS coated fibers were slightly different from that of HGNS in solution phase. A red shift in the peak wavelength with a slight broadening of the spectrum was noticed (Fig. 7c). An average red shift of 26 ± 3 nm (n = 10) was observed. This is attributed to near-field plasmon coupling between the immobilized HGNS with the interparticle gap less than ~2.5 times the particle diameter.[45] A similar behavior was reported earlier after coating gold nanoparticles on sensing surfaces.[33,46] Further, to verify the interparticle distance, FEG-SEM imaging of HGNS coated fiber-optic probes was carried out.

Fig. 8 shows the FEG-SEM images of HGNS coated fiber-optic probe captured at different magnifications. The HGNS were found to be present homogeneously on fiber-optic probes (Fig. 8a). The hollow cavities were easily noticeable in immobilized nanostructures at high magnification (Fig. 8b). A very few clusters comprising of 6-10 HGNS were also observed. HGNS coverage was determined by calculating the area covered by two-dimensional projection of the HGNS on the surface divided by the total area of the surface. The mean density and percent coverage of HGNS were found to be 32 ± 3 nanoparticles/μm^2 and 12.3 ± 1.3 respectively. The interparticle distance among some of the immobilized HGNS was found to be less than 2.5 times of their diameter, which might have resulted in plasmon coupling. As a result, a red shift in plasmonic wavelength and broadening of the absorption spectra was observed during HGNS binding of fiber probe.

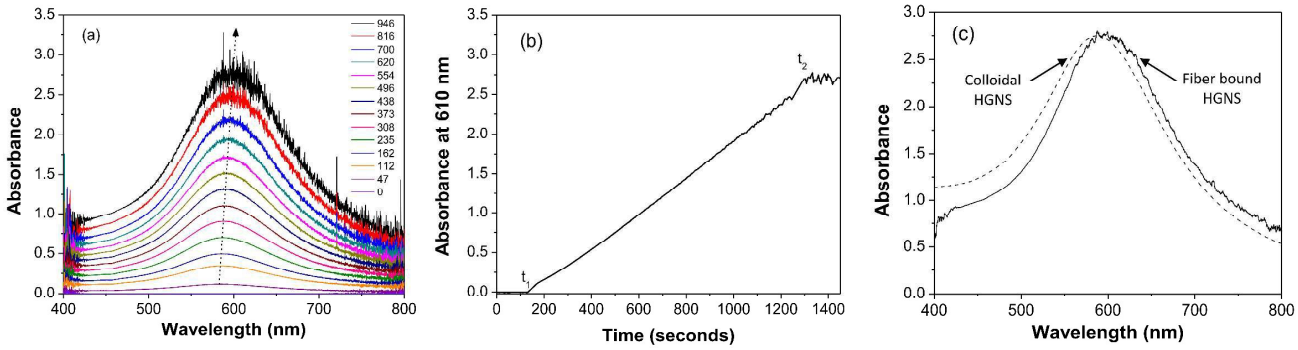

Fig. 7 a) Absorbance spectra recorded at different absorbance values during the process of binding of HGNS on dendrimer functionalized fiber-optic probe. Arrow indicates the red shift in the peak absorbance wavelength with the increase in binding of HGNS on fiber-optic probe; b) Kinetic curve showing the linear response of HGNS binding on fiber-optic probe. The probe was exposed to HGNS dispersion at time point 't_1' while the flow cell was flushed with DI water at time point 't_2' to prevent the further binding of HGNS; c) Comparison of absorbance spectrum obtained from fiber-optic probe due to HGNS binding (solid line) with that of colloidal solution of HGNS (dashed line). Note: Absorbance spectrum of colloidal solution of HGNS was normalized to absorbance intensity of HGNS immobilized fiber-optic probe to illustrate shift in peak plasmonic wavelength after HGNS binding.

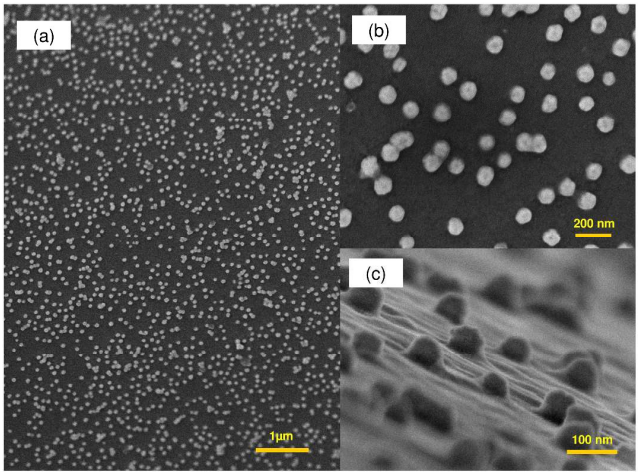

Fig. 8 FEG-SEM image of HGNS immobilized optical fiber surface at a) low magnification (×10000) and b) high magnification (×75000) shows the uniform distribution of HGNS on fiber surface. A small dark spot in the centre of HGNS represents the hollow cavity; c) High resolution (×150000) side view of HGNS immobilized optical fiber probe.

HGNS coated fiber-optic probes were evaluated for bulk RI sensitivity using sucrose solution of different RI. Fig. 9a shows the absorbance spectra obtained after exposing the HGNS coated sensor probe with sucrose solutions of different RI. A significant change in absorbance intensity (along with shift in peak absorption wavelength) was observed for different RI solutions.[46] This was attributed to the refractive loss of the propagating rays in optical fiber probe due to change in effective RI in the sensing region.[34] The detection range was found to be linear in the range from 1.33 to 1.36 RIU in aqueous phase. Refractive index sensitivity, defined as the ratio of the change in absorbance to the change in RI was found to be linear between 1.33 and 1.36 RI as shown in Fig. 9b ($R^2 = 0.99$). The RI Sensitivity was found to be 47.3 ± 2.9 ΔA_{640nm}/RIU (n = 3). The sensitivity of HGNS based probe was found to be 1.5 fold better than the solid gold nanoparticles (size = 40 nm, λ_{max} = 535 nm) based fiber-optic sensor of similar configuration.[33] Compared to a tip based LSPR sensor, having a film of gold nanoparticles (size = 47 nm), HGNS anchored U-shaped fiber-optic sensor showed improved sensitivity, close to five-fold.[47]

Biosensor application

The absorbance spectra and kinetic curve obtained from the binding of HIgG molecules on HGNS coated fiber-optic probe are shown in Fig S-4. The binding of HIgG followed a first order kinetic curve with initial rapid binding followed by slower rate and finally a plateau. A similar kinetics of bioreceptor binding has also been observed earlier using different techniques.[48,49] After HIgG binding, the peak absorption wavelength appeared at 640 nm constituting a red shift of ~27 nm as compared to HGNS coated fiber-optic probes. This is due to the increase in effective RI of the nano-environment surrounding the HGNS (i.e. the sensing region), produced by the binding of MUA-SAM and HIgG molecules. This might also be the result of more effective interparticle coupling at higher RI. An analogous red shift has also been reported during IgG immobilization on functionalized gold nanorods.[47,50]

HIgG immobilized HGNS (HIgG-HGNS) coated fiber probes were used to detect different concentrations of GaHIgG. Prior to

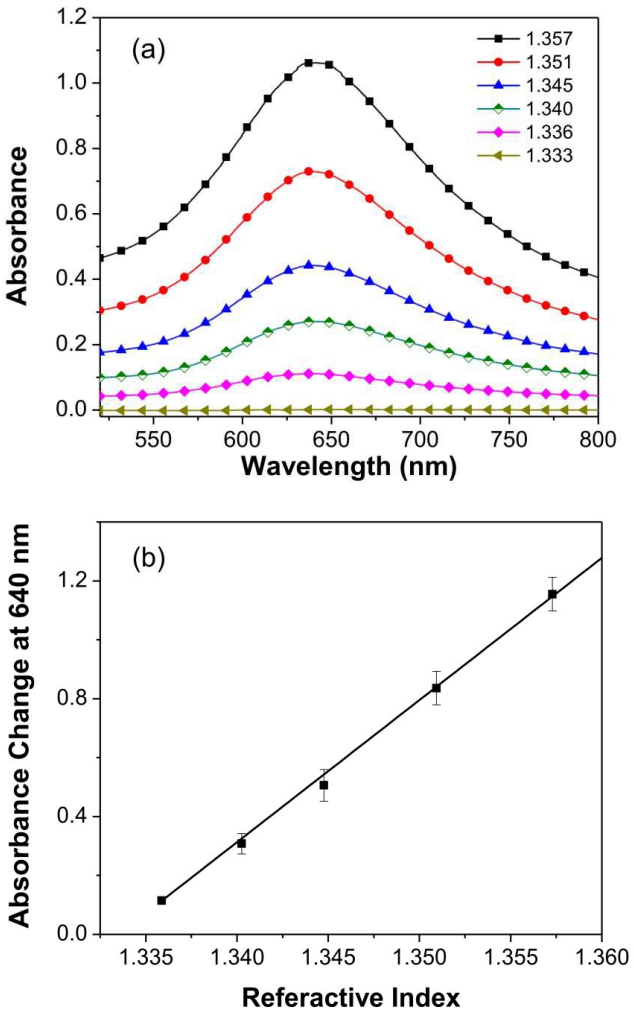

Fig. 9 Absorbance spectra obtained from HGNS coated U-shaped fiber-optic probe in the presence of sucrose solution of different refractive indices. Deionized water (RI = 1.333) was taken as reference; b) Sensitivity of HGNS bound U-shaped probes to RI changes at the probe surface between 1.33 and 1.36. A linear fit for the absorbance responses obtained for the probe resulted in a slope or sensitivity of 47.3 with R^2 = 0.99.

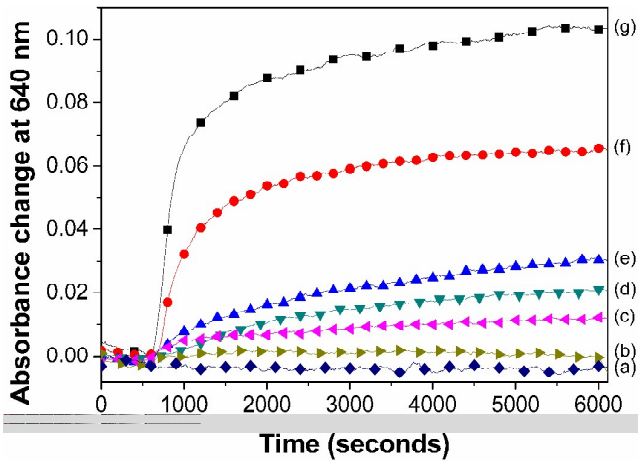

Fig. 10 Time-resolved absorbance response obtained from HIgG-HGNS coated fiber-optic probes when incubated with different concentrations of GaHIgG analyte solution, a) no analyte is added to check the stability of HIgG-HGNS coated fiber probes, b) 1 ng/mL, c) 10 ng/mL d) 100 ng/mL, e) 3 μg/mL, f) 10 μg/mL and g) 15 μg/mL.

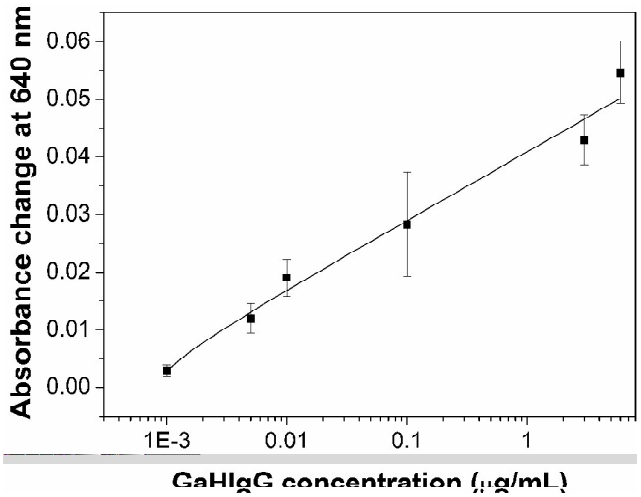

Fig. 11 Dose response curve obtained from the binding of various concentrations of GaHIgG analyte to HIgG-HGNS coated fiber-probes. (n = 3 for each concentration).

this, HIgG-HGNS coated probes were treated with BSA solution to block the free activated sites. Fig. 10 shows the real-time absorbance changes (at λ_{max} = 640 nm) obtained from HIgG-HGNS coated fiber-optic probes when incubated with different concentrations of GaHIgG. It is important to note that a substantial rise in the absorbance value was observed in the first five minutes after introduction of GaHIgG analyte solution in the flow cell as compared to the control sample. This suggests that this sensor can detect analyte within five minutes. However, a saturated or steady state response was obtained after 90 mins of incubation. A similar pattern of increase in absorbance was also observed in earlier reports incorporating a similar sensing configuration, throughout the detection phase.[33] This indicates that at low analyte concentration, the immunoreaction is diffusion rate limited. In contrast, at high analyte concentration (≥10 μg/mL), the sensor response increased rapidly during initial binding which was followed by a slow binding rate. This suggests that most of the available bioreceptors are saturated in 10-15 min and reached to the nearly equilibrium state. The semi-logarithmic plot of the dose-response curve, i.e. change in absorbance as a function of analyte concentration, showed a good linearity in the concentration range between 1 ng/mL to 6 μg/mL (R^2 ~ 0.98) (Fig. 11).

The HGNS coated U-shaped fiber-probes were easily capable of detecting analyte concentration of 10 ng/mL (~70 pM). The limit of detection is an order lower than that reported in with GNP based fiber-optic sensors of similar geometry[33] and nanoSPR chips.[46] Also, the HGNS based sensor showed one- and four-orders better sensitivity compared to gold bipyramid nanoparticles[10] and silica gold nanoshells[51] based immunosensors, respectively. The limit of detection (LOD) of HGNS based biosensor was found comparable with the core-shell nanostructures based LSPR chips developed by Endo *et al.* (2008).[52] However, fabrication of these core-shell nanostructures based LSPR chips involves a number of processing steps, costly instruments and controlled environment than that of HGNS based fiber-optic probes. Thus, HGNS based sensor fabrication on an optical fiber platform, has the advantages of low-cost and possibility of rapid manufacturing.

To test the non-specific binding, HGNS coated sensor probes were immobilized with rabbit IgG using the protocol as explained above in this section. Absorbance response was monitored in real-time for 10 μg/mL concentration of GaHIgG analyte solution. A very small change in absorbance was measured, which corresponds to ~10% of the signal for the specific binding of 10 μg/mL of GaHIgG to HIgG (See ESI, Fig. S4†). This might be due to a low level of nonspecific binding of proteinaceous analyte on the sensor surface.

Conclusion

We have demonstrated the synthesis of uniform and monodispersed hollow gold nanostructures. The preparation method involved three simple steps, i) gold seed synthesis, ii) heteroepitaxial synthesis of silver nanospheres and iii) galvanic replacement reaction between AgNS and gold salt solution. The main advantage of the developed method is the room temperature synthesis without any prior treatment of gold salt. The size and peak absorbance wavelength could be readily tuned by adjusting the molar ratio of gold salt to AgNS. The consistency of particle shape and size was reflected in the optical properties, which inspired the development of a label-free LSPR based sensor. The HNGS based fiber-optic sensor showed a 1.5 fold enhancement in sensitivity compared to GNP based LSPR sensors. Finally, these HGNS based fiber-optic probes were used to develop immunosensors, which showed one- to four-orders better limit of detection compared to other gold nanostructures based biosensors. Overall, the method of HGNS synthesis described here will provide, three major advantages over previous systems: (i) their plasmon resonance peaks and sizes can be conveniently tuned by controlling only one parameter, i.e. the gold to silver molar ratio; (ii) the reaction is uniform and the resultant nanostructures are monodispersed; (iii) their surfaces can be readily engineered with various functional groups for diagnostics and other applications by taking advantage of the well-established gold-thiolate monolayer chemistry.

Acknowledgements

The authors gratefully acknowledge the Sophisticated Analytical Instrument Facility (SAIF), and IIT-Bombay central facility (FEG-SEM and FEG-TEM) for characterization studies. The authors thank Nirmal S. Punjabi for his help in data analysis.

Notes and references

[a] *Department of Biosciences and Bioengineering, IIT Bombay, Mumbai 400 076, India.*
[b] *School of Bio Sciences and Technology, VIT University, Vellore, Tamilnadu, 632 014, India.*
[c] *Centre of Excellence for Nanoelectronics, IIT Bombay, Mumbai 400 076, India.*
[d] *Centre for Research in Nanotechnology and Science, IIT Bombay, Mumbai 400 076, India*
** Corresponding author: mukherji@iitb.ac.in (S. Mukherji); Fax: +91 22 2572 3480; Tel: +91 22 2576 776*

† Electronic Supplementary Information (ESI) available: Method of gold seed particle synthesis; Extinction spectrum and FEG-TEM image of gold seed particles; chemical reactions involved in the preparation diamine silver complex; Extinction spectra, FEG-TEM image and histogram of silver nanoparticles produced from heteroepitaxial growth method using

gold seeds; reagents and their compositions used to produce different batches of HGNS; method for TEM grid preparation for HGNS samples; detail about the optical set-up; absorbance changes obtained from the binding of GaHIgG to nonspecific Rabbit-IgG-HGNS coated U-shaped fiber probes. [details of any supplementary information available should be included here]. See DOI: 10.1039/b000000x/

References

1 E. Hutter and J. H. Fendler, *Advanced Materials*, 2004, **16**, 1685.
2. K. A. Willets and R. P. Van Duyne, *Annual Review of Physical Chemistry*, 2007, **58**, 267.
3. J. N. Anker, W. P. Hall, O. Lyandres, N. C. Shah, J. Zhao and R. P. Van Duyne, *Nature Materials*, 2008, **7**, 442.
4. K. M. Mayer and J. H. Hafner, *Chemical Reviews*, 2011, **111**, 3828.
5. C. D. Chen, S. F. Cheng, L. K. Chau and C. R. C. Wang, *Biosensors and Bioelectronics*, 2007, **22**, 926.
6. G. J. Nusz, A. C. Curry, S. M. Marinakos, A. Wax and A. Chilkoti, *ACS Nano*, 2009, **3**, 795.
7. T. Endo, S. Yamamura, N. Nagatani, Y. Morita, Y. Takamura and E. Tamiya, *Science and Technology of Advanced Materials*, 2005, **6**, 491.
8. H. M. Hiep, T. Endo, K. Kerman, M. Chikae, D. K. Kim, S. Yamamura, Y. Takamura and E. Tamiya, *Science and Technology of Advanced Materials*, 2007, **8**, 331.
9. S. K. Dondapati, T. K. Sau, C. Hrelescu, T. A. Klar, F. D. Stefani and J. Feldmann, *ACS Nano*, 2010, **4**, 6318.
10. S. Lee, K. M. Mayer and J. H. Hafner, *Analytical Chemistry*, 2009, **81**, 4450.
11. K. M. Mayer, F. Hao, S. Lee, P. Nordlander and J. H. Hafner, *Nanotechnology*, 2010, **21**, 255503.
12. S. E. Skrabalak, J. Chen, L. Au, X. Lu, X. Li and Y. Xia, *Advanced Materials*, 2007, **19**, 3177.
13. J. Satija, R. Bharadwaj, V. V. R. Sai and S. Mukherji, in *Nanotechnology Science and Applications,* 2010, **3**, 171.
14. V. Vongsavat, B. M. Vittur, W. W. Bryan, J. H. Kim and T. R. Lee, *ACS Applied Materials & Interfaces*, 2011, **3**, 3616.
15. M. A. Mahmoud and M. A. El-Sayed, *Journal of the American Chemical Society*, 2010, **132**, 12704.
16. Y. Sun and Y. Xia, *Nano Letters*, 2003, **3**, 1569.
17. B. G. Prevo, S. A. Esakoff, A. Mikhailovsky and J. A. Zasadzinski, *Small*, 2008, **4**, 1183.
18. J. W. Hu, Y. Zhang, J. F. Li, Z. Liu, B. Ren, S. G. Sun, Z. Q. Tian and T. Lian, *Chemical Physics Letters*, 2005, **408**, 354.
19. L. Chen, W. Zhao, Y. Jiao, X. He, J. Wang and Y. Zhang, *Spectrochimica Acta Part A: Molecular and Biomolecular Spectroscopy*, 2007, **68**, 484.
20. Y. Sun, B. Mayers and Y. Xia, *Advanced Materials*, 2003, **15**, 641.
21. J. Chen, F. Saeki, B. J. Wiley, H. Cang, M. J. Cobb, Z. Y. Li, L. Au, H. Zhang, M. B. Kimmey, Xingde and Y. Xia, *Nano Letters*, 2005, **5**, 473.
22. A. M. Schwartzberg, T. Y. Oshiro, J. Z. Zhang, T. Huser and C. E. Talley, *Analytical Chemistry*, 2006, **78**, 4732.
23. M. Rycenga, C. M. Cobley, J. Zeng, W. Li, C. H. Moran, Q. Zhang, D. Qin and Y. Xia, *Chemical Reviews*, 2011, **111**, 3669.
24. D. G. Duff, A. Baiker and P. P. Edwards, *Langmuir*, 1993, **9**, 2301.
25. B. Nikoobakht and M. A. El-Sayed, *Chemistry of Materials*, 2003, **15**, 1957.
26. Y. G. Kim, S. K. Oh and R. M. Crooks, *Chemistry of Materials*, 2003, **16**, 167.
27. R. Dondi, W. Su, G. A. Griffith, G. Clark and G. A. Burley, *Small*, 2012, **8**, 770.
28. J. Soukupová, L. Kvítek, A. Panáček, T. Nevěčná and R. Zbořil, *Materials Chemistry and Physics*, 2008, **111**, 77.
29. Y. Sun and Y. Xia, *Journal of the American Chemical Society*, 2004, **126**, 3892.
30. B. D. Gupta, H. Dodeja and A. K. Tomar, *Opt Quant Electron*, 1996, **28**, 1629.
31. A. Leung, P. M. Shankar and R. Mutharasan, *Sensors and Actuators B: Chemical*, 2007, **125**, 688.
32. S. Srivastava, V. Arora, S. Sapra and B. Gupta, *Plasmonics*, 2012, **7**, 261.
33. V. V. R. Sai, T. Kundu and S. Mukherji, *Biosensors and Bioelectronics*, 2009, **24**, 2804.
34. J. Satija, N. Punjabi, V. V. R. Sai and S. Mukherji, *Plasmonics*, 2014, **9**, 251.
35. S. Pathak, A. K. Singh, J. R. McElhanon and P. M. Dentinger, *Langmuir*, 2004, **20**, 6075.
36. J. Satija, V. V. R. Sai and S. Mukherji, *Journal of Materials Chemistry*, 2011, **21**, 14367.
37. V. Gajbhiye and N. K. Jain, *Biomaterials*, 2011, **32**, 6213.
38. C. Y. Chiang, M. L. Hsieh, K. W. Huang, L. K. Chau, C. M. Chang and S. R. Lyu, *Biosensors and Bioelectronics*, 2010, **26**, 1036.
39. H. Ogi, Y. Fukunishi, H. Nagai, K. Okamoto, M. Hirao and M. Nishiyama, *Biosensors and Bioelectronics*, 2009, **24**, 3148.
40. M. Yang, R. N. Alvarez-Puebla, H. S. Kim, P. Aldeanueva-Potel, L. M. Liz-Marzán and N. A. Kotov, *Nano Letters*, 2010, **10**, 4013.
41. X. Lu, L. Au, J. McLellan, Z. Y. Li, M. Marquez and Y. Xia, *Nano Letters*, 2007, **7**, 1764.
42. L. Au, X. Lu and Y. Xia, *Advanced Materials*, 2008, **20**, 2517.
43. X. Liu, M. Atwater, J. Wang and Q. Huo, *Colloids and Surfaces B: Biointerfaces*, 2007, **58**, 3.
44. J. P. Conzen, J. Bürck and H. J. Ache, *Appl. Spectrosc.*, 1993, **47**, 753.
45. K. H. Su, Q. H. Wei, X. Zhang, J. J. Mock, D. R. Smith and S. Schultz, *Nano Letters*, 2003, **3**, 1087.
46. N. Nath and A. Chilkoti, *Analytical Chemistry*, 2004, **76**, 5370.
47. H. H. Jeong, N. Erdene, S. K. Lee, D. H. Jeong and J. H. Park, *Optical Engineering*, 2011, **50**, 124405.
48. X. Liu and W. Tan, *Analytical Chemistry*, 1999, **71**, 5054.
49. H. Nygren, *Biophysical Chemistry*, 1994, **52**, 45.
50. K. M. Mayer, S. Lee, H. Liao, B. C. Rostro, A. Fuentes, P. T. Scully, C. L. Nehl and J. H. Hafner, *ACS Nano*, 2008, **2**, 687.
51. Y. Wang, W. Qian, Y. Tan and S. Ding, *Biosensors and Bioelectronics*, 2008, **23**, 1166.
52. T. Endo, S. Yamamura, K. Kerman and E. Tamiya, *Analytica Chimica Acta*, 2008, **614**, 182.

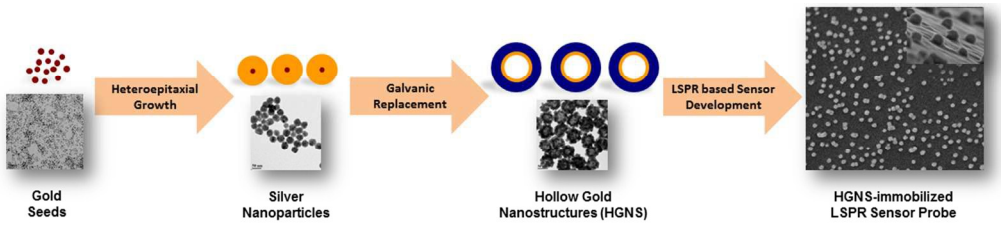

319x69mm (96 x 96 DPI)